Atmos. Meas. Tech. Discuss., 6, 6935–6974, 2013
www.atmos-meas-tech-discuss.net/6/6935/2013/
doi:10.5194/amtd-6-6935-2013

Atmospheric Measurement Techniques Discussions

A new experimental approach to study the hygroscopic and the optical properties of aerosols: application to ammonium sulfate particles

C. Denjean, P. Formenti, B. Picquet-Varrault, Y. Katrib, E. Pangui, P. Zapf, and J. F. Doussin

Laboratoire Interuniversitaire des Systèmes Atmosphériques (LISA), UMR7583, CNRS, Université Paris-Est-Créteil (UPEC) et Université Paris Diderot (UPC), Institut Pierre Simon Laplace (IPSL), Créteil, France

Received: 10 June 2013 – Accepted: 18 July 2013 – Published: 29 July 2013

Correspondence to: C. Denjean (cyrielle.denjean@lisa.u-pec.fr)

Published by Copernicus Publications on behalf of the European Geosciences Union.

Abstract

A new methodology for the determination of size distribution and optical properties of aerosols as a function of the relative humidity (RH) in simulation chamber is described. The hygroscopic properties of aerosols can be investigated by exposing aerosols to varying RH ranging from 0 to 100 % for approximately 1 h. This method is also proved useful in both providing information on the RH dependence of size and scattering coefficient (σ_{scat}) of the overall size distribution. The complex refractive index (CRI) of aerosols can be retrieved at λ = 525 nm, as well as in the visible spectrum. Ammonium sulfate particles that have well known optical and hygroscopic properties were used for the measurements. The particle's growth was compared to values obtained for one selected size of particles (150 nm) with a H-TDMA and the effect of the residence time for particles humidification was investigated. The CRI of ammonium sulfate particles obtained from the two methods (1.54–1.57) compared favorably to each other and are also in reasonable agreement with the literature values. When the humidification is performed in the chamber for a few minutes, a continuous increase of the ammonium sulfate particle's size and σ_{scat} was observed from RH values as low as 30 % RH. Comparison of the measured and modeled values based on Köhler and Mie theories shows that layers of water are adsorbed on ammonium sulfate particles below the deliquescence point. In contradiction, the particle's growth reported with H-TDMAs showed a prompt deliquescence of ammonium sulfate particles with no continuous growth in size at low RH. The findings highlight the need to allow sufficient time for particle-water vapor equilibrium in investigating the aerosols hygroscopic properties. H-TDMA instruments induce limited residence time for humidification and seem to be insufficient for water adsorption on ammonium sulfate particles.

AMTD
6, 6935–6974, 2013

1 Introduction

Atmospheric aerosols play an important role in the Earth's climate through their effect on the radiative budget, the atmospheric chemistry and precipitation. They influence the Earth's radiative budget by absorbing and scattering incoming solar radiation and outgoing terrestrial radiation (direct effect) (Haywood et al., 1998; Charlson et al., 1992; Forster et al., 2007), but also by altering cloud properties by acting as cloud condensation nuclei (CCN) and thereby modifying cloud albedo, lifetime and precipitation (indirect effect) (Hansen et al., 1997; Albrecht, 1989; Lohmann and Feichter, 2005).

In order to evaluate the impact of atmospheric aerosols, it is important to understand the complex influence of the aerosol size and chemical composition on the optical properties. The ability of aerosols to interact with light is determined by their optical properties, strong functions of both the particle's size and chemical composition. The chemical composition determines the complex refractive index (CRI) ($m = n + ik$), which describes the scattering (real part n) and absorbing (imaginary part k) characteristics of a substance. The CRI is a major parameter to determine factors relevant to radiative transfer, such as single scattering albedo, asymmetry factor and efficiency of light extinction.

There are several means to measure the CRI of atmospheric aerosols. Nakayama et al. (2010) estimated the CRI in closure experiments based on measured particle size dependence of the extinction and scattering coefficients (σ_{ext} and σ_{scat}) together with Mie–Lorenz theory. This method uses instruments based on monochromatic radiation and thus allows the determination of CRI at specific wavelength. Due to a lack of data measured in the visible spectrum, a new approach which combines measurements of aerosol size distributions with two measurement techniques, that depends on a different aerosol property, has been recently introduced by Flores et al. (2009) and Wex et al. (2009). A white light aerosol Optical Particle Counter (OPC) was installed downstream a Differential Mobility Analyzer (DMA) to retrieve the particle's CRI. The OPC measures the particle optical size, which depends on their CRI, while the DMA

AMTD
6, 6935–6974, 2013

measures a mobility diameter that is a geometric diameter when spherical particles are assumed. These instruments operate over different size ranges, but overlap does occur between them. The CRI was determined based on the superposition of size distributions obtained from the DMA and those calculated from the OPC response to CRI. One of the major limitations in retrieving CRI with this method was the small size region used in the data reconciliation. The determination of the CRI was constrained to particles size corresponding to the region of overlap between instruments.

The aerosol properties are strongly dependent on atmospheric conditions, in particular the relative humidity (RH) of ambient air. The interaction of particles with water is associated with changes in their size and their chemical composition, thereby modifying their potential to act as cloud condensation nuclei, their chemical reactivity, their scattering efficiencies and, in a lesser degree, their absorbing efficiencies (Orr Jr. et al., 1958; Hegg et al., 1993; Nemesure et al., 1995; Martin, 2000). Thus, laboratory quantification of the RH dependence of size and light scattering is necessary for inclusion into radiative transfer calculations (Charlson et al., 1992; Haywood and Ramaswamy, 1998; Hegg et al., 1993; Nemesure et al., 1995).

Previous laboratory studies have measured the change in particle diameter after particle hygroscopic growth (Cruz and Pandis, 2000; Hämeri et al., 2000; Prenni et al., 2003). Hygroscopic Tandem Differential Mobility Analyzers (H-TDMA) have been extensively used to determine the size growth factor (GF) of particles, i.e. the ratio of the particle diameter at a given RH to the particle diameter under low RH condition (Biskos et al., 2006; Swietlicki and Hansson, 2008; Prenni et al., 2003; Hämeri et al., 2000; Cruz and Pandis, 2000). This GF can be used to derive the number of CCN with Köhler theory (Petters et al., 2008; Huff Hartz et al., 2005). A limitation of H-TDMA is that measurements of GF are usually performed for single size of particles because measurements for several classes of size are time consuming. The study performed by Biskos et al. (2006) has shown that GF depends on the size of particles. Hence, it has been observed that for similar chemical composition, nanoparticles exhibit smaller GF because the relative contribution of the surface term to the free energy of a particle

AMTD
6, 6935–6974, 2013

increases markedly for particles smaller than 100 nm. Thus, the GF has to be explored through measurement of the alteration of polydisperse aerosol size distribution after water uptake.

Model calculations on the direct radiative effect require also data on the influence of RH on σ_{scat} (Charlson et al., 1992). Mie scattering theory has been used in the past to calculate the RH dependence of light scattering using GF of many inorganic compounds (Garland et al., 2007; Beaver et al., 2008; Wex et al., 2005). However, because of a lack of optical and thermodynamic data for many organic compounds, the change in σ_{scat} due to water uptake is not fully predicted (Malm et al., 2005; Saxena et al., 1995). As a consequence, direct measurements of the f(RH), i.e. the ratio of σ_{scat} at some RH to the σ_{scat} under low RH condition, have been monitored using controlled RH nephelometers (Kus et al., 2004; Covert et al., 1972; Yoon and Kim, 2006; ten Brink et al., 2000). These measurements provide an integrated growth measurement of the overall size distribution.

An important concern in measuring the hygroscopic properties of the particles is to allow sufficient time for particle-water vapor equilibrium. Until now, field H-TDMA and controlled RH nephelometers studies have assumed that a residence time of a few seconds is long enough to allow particles to reach their equilibrium size (Villani et al., 2008; Nilsson et al., 2009; Kus et al., 2004). However, various studies have discussed the possibility that it is not the case (Chan and Chan, 2005; Saxena et al., 1995; Duplissy et al., 2009). This could result in an underestimation of the water content and size of particles. For example, Ristovski et al. (1998) found with a H-TDMA that the GF of 50 nm dry NaCl particles was 1.9 for a residence time of 7.4 s, instead of 1.1 for a shorter residence time of 2.2 s. Thus, it is desirable to investigate the effect of the residence time for particles humidification.

Simulation chamber experiments are very useful to produce data on the physical-chemical, optical and hygroscopic properties of specific aerosols under various meteorological conditions. It allows the study of the aerosol formation and the simulation of

AMTD
6, 6935–6974, 2013

its evolution during the atmospheric transport by controlling the oxidative and photolytic environment (Meyer et al., 2008; Henry and Donahue, 2012; Tritscher et al., 2011).

This work describes a new method for the simultaneous measurement of aerosol size and optical properties of aerosols and their variation with RH in a simulation chamber. In order to study the aerosol optical properties, the CRI was retrieved at a specific wavelength, as well as in the visible spectrum. The hygroscopic behavior of aerosols was investigated by measuring the RH dependence of size and σ_{scat} of the overall size distribution up to 100 % RH. Measured GF were compared to values obtained with an H-TDMA and the effect of the residence time for particles humidification was investigated. Ammonium sulfate particles were studied, as it is a common component in the atmosphere and efficient scatter of solar radiation (Charlson et al., 1992). Both the optical and hygroscopic properties of these particles were intensively studied in the past (Tang, 1996; Cruz and Pandis, 2000; Gysel et al., 2001; Dinar et al., 2008; Riziq, 2006; Flores et al., 2009). Therefore, this aerosol is well suited for the validation of our methodology.

2 Measurements

2.1 Smog chamber set-up

The CESAM chamber (French acronym for Experimental Multiphasic Atmospheric Simulation Chamber) is designed to allow research in multiphase atmospheric (photo)-chemistry which involves both gas phase and condensed phase processes including aerosol and cloud chemistry. The chamber is described in detail elsewhere (Wang et al., 2011), but characteristics relevant to this study are reported here. CESAM consists of a 4.2 m^3 stainless steel chamber. Aerosols exhibit a lifetime long enough to study aerosol aging over several hours or days, depending on the aerosol size distribution. CESAM has the potential to vary in situ the RH of the reaction mixture by adding water vapor in the reactor. Both temperature and RH are measured with a HMP234

AMTD
6, 6935–6974, 2013

Vaisala humidity and temperature transmitter equipped with a capacitive thin-film sensor Humicap. The sensor was recently factory calibrated prior to the experiments and has an RH accuracy of ±1.9 % up to 90 % RH and a temperature accuracy of ±0.1 °C at 20 °C.

Figure 1 shows a schematic of the experimental setup to measure aerosol properties.

A white light aerosol OPC (Welas, Palas, model 2000) was used to determine the number size distribution of particles with diameters above 300 nm by measuring the pulse of scattered white light. The white light spectrum is spanned from 370 to 780 nm. The OPC was calibrated using a calibration dust (standard CalDust 1100) which has the same CRI as polystyrene latex (PSL).

A scanning mobility particle sizer (SMPS) that includes a differential mobility analyzer (DMA, TSI model 3080) interfaced to a condensation particle counter (CPC, TSI model 3010) was used to monitor sub-micrometer particle number size distribution. The DMA was operated at flow rates 3/0.3 Lpm (sheath flow/aerosol sample flow). The aerosol sample flow is set by the CPC with a nominal flow rate of 0.3 Lpm. The resulting measured size distribution ranged between 14 to 505 nm. For its RH control, the DMA exhibits the same set-up as the DMA2 of the H-TDMA and will be described in details in Sect. 2.2. The size calibration of the SMPS was performed using several sizes of monodisperse PSL particles (Duke Scientific). PSL diameters ranging from 100 to 500 nm were produced with a constant output atomizer (TSI model 3075).

The aerosol scattering coefficient was measured using an integrating nephelometer (model M9003, Ecotech). This instrument has a LED that provides light at 525 nm wavelength. The light scattered by the particles is collected with a photomultiplier at scattering angles between 10° and 170° (Liu et al., 2008). The nephelometer was calibrated with filtered air and CO_2 separately. The sample air is usually drawn by a fan through the sample inlet into the measurement volume. Because our experiments were carried out at a pressure 3 mbar greater than the atmospheric pressure, the circulating air system of the nephelometer does not allow the flowrate control. Thus, the fan was replaced by an external pump working at 3 Lpm. The temperature was measured

AMTD
6, 6935–6974, 2013

both at the sample inlet and within the cell of the nephelometer with an accuracy of ±0.6 °C, and the RH was measured within the cell of the nephelometer with an accuracy of ±3 %. The nephelometer RH sensor and the SMPS RH sensors were calibrated in the CESAM chamber by varying the RH from 0 to 100 % and using as a reference the CESAM sensor that was recently factory calibrated. The intercomparison of the temperature sensors shows a good agreement within uncertainties.

The aerosol light absorption coefficient was derived from the aerosol light attenuation measured with an aethalometer (Model AE31, Magee Scientific). The aethalometer measures the optical attenuation of light transmitted through the aerosols deposited continuously on a quartz fiber filter. It operates with several light sources at seven wavelengths covering the near ultra-violet to the near infrared wavelength range (λ = 370, 470, 520, 590, 660, 880 and 950 nm). It has been observed that the aethalometer can suffer from biases at high RH as a result of filter taking up water and scattering more light compared to the reference measurement (Cappa et al., 2008; Arnott et al., 2005). Therefore, the aethalometer was not used during the humidification of aerosols.

2.2 Development of a H-TDMA

In order to measure the water uptake of monodisperse particles, a H-TDMA has been developed. H-TDMAs were firstly introduced by Liu et al. (1978) and are used worldwide in laboratories (Meyer et al., 2008; Prenni et al., 2003; Saathoff et al., 2003; Varutbangkul et al., 2006) and during field campaigns (Saxena et al., 1995; Sjogren et al., 2007; Svenningsson et al., 1992). They are composed of two DMAs in series, an aerosol humidifier in between and a CPC. A diagram of the layout of the HTDMA is shown in Fig. 2.

The dry aerosol passes through a diffusion charger (^{85}Kr) to reach a bipolar charge distribution and an initial mobility diameter is selected with a first DMA. The resulting monodisperse aerosol then passes through a humidifier at a well-defined RH, and a second DMA coupled to a CPC measures the wet size distribution over mobility diameter. In this study, both DMAs are TSI 3080 types operating at flow rates 3/0.3 Lpm

AMTD
6, 6935–6974, 2013

(sheath flow/aerosol sample flow) and the CPC (TSI 3075) was set at 0.3 Lpm. A closed loop recirculation was used for the sheath flow in DMA in order to avoid problem of stabilizing the RH. As for the SMPS set-up, the sheath air hydrophilic filter was replaced by a hydrophobic filter (Whatman, model 6702-7500). This procedure avoids RH gradients and particle size changes inside the DMA.

The residence time of particles for humidification is equal to the residence time in the RH conditioner (10 s) plus the transit time in the second DMA (5 s). This is generally sufficiently long for particles to reach their equilibrium with water vapor (Chan and Chan, 2005; Saxena et al., 1995; Duplissy et al., 2009).

The RH of the DMA2 is monitored at both the inlet and outlet with capacitive RH sensors (Vaisala, model HMP-50) placed in the aerosol sample, sheath, and excess air. The sensors have an accuracy of ±3 % up to 90 % RH. They also measure the temperature with an accuracy of ±0.6 °C at 20 °C. Great attention has been paid to the calibration of the sensor, as it is a key parameter for the RH control in the DMA column. The RH of sheath and aerosol flows are separately adjusted to the desired value by passing through a multiple-tube Nafion conditioner (Permapure, model PD-50T). Water saturated air is generated by bubbling high-purity water (18.2 MΩ, ELGA Maxima). The humidification for both the aerosol and the sheath flows is controlled by a proportional-integral-derivative (PID) controller programmed using LabVIEW™ which provides feedback to the RH sensors and thereby adjusts the bubbling rate. The sheath flow is humidified at the same RH as the aerosol sample flow to avoid RH gradients in the DMA2. The temperature can have significant influence on RH, especially at high RH. Here, the H-TDMA is not directly controlled in temperature, but a specific attention was given to prevent drafts and keep temperature of the room stable. Tests were performed to evaluate the system ability to maintain a stable humidity. The RH set point was set at a constant value of 90 % during 5 h. In this way, the measured RH was within ±2 % of the target value (RH uncertainties are ±3 % RH for 10 % ≤ RH ≤ 90 %).

AMTD
6, 6935–6974, 2013

2.3 Simulation chamber operation

Before each experiment, the chamber was cleaned by pumping at a secondary vacuum (4×10^{-4} mbar) overnight. The chamber was filled with a synthetic air produced from the mixture of 200 mbar of oxygen (Air Liquide, Alphagaz class 1, purity 99.9 %) and 800 mbar of nitrogen produced from the evaporation of a pressurized liquid nitrogen tank. The background aerosol concentration was below 0.1 $\mu g\,m^{-3}$. Particles were generated from 0.03 M ammonium sulfate solution using a constant output atomizer (TSI, model 3075). The particles were next passed through a diffusion dryer (TSI, model 3062) which reduced the RH, and introduced to the chamber. At the injection, the RH in the chamber was much lower than 1 % which further helped to dry out the particles. The initial starting conditions of all conducted experiments are summarized in Table 1.

The size, the optical properties and the water uptake of monodisperse aerosols (as measured with the H-TDMA) were measured under dry conditions after the mass of ammonium sulfate particles reached a maximum in the chamber. At the end of the experiments, the hygroscopicity of polydisperse particles were investigated by injecting water vapor produced in a small glass vessel filled with ultrapure water (18.2 MΩ, ELGA Maxima) which is located below the chamber and directly connected to it. The RH in the chamber increased linearly from 0 to 100 % in approximately 1 h. The SMPS, the OPC and the nephelometer were used to follow in-situ the variation in number size distribution and σ_{scatt} as a function of relative humidity.

3 Data analysis

3.1 Determination of the Complex Refractive Index

The optical properties of dry ammonium sulfate particles were established by retrieving its CRI using two different methods.

AMTD
6, 6935–6974, 2013

The ammonium sulfate CRI at 525 nm was firstly derived by optical closure experiments involving σ_{scat} and σ_{abs} measured at 525 nm and the number size distribution also determined experimentally. σ_{scat} and σ_{abs} were also calculated according to the following equation:

$$\sigma_{\text{scat, abs}}(\lambda, m) = \sum_{D_p} Q_{\text{scat, abs}}(D_p, \lambda, m) \frac{\pi}{4} D_p^2 \left(\frac{dN}{d\log D_p} \right) d\log D_p \quad (1)$$

where D_p is the geometrical particle diameter, $\frac{dN}{d\log D_p}$ the number size distribution and $Q_{\text{scat, abs}}(D_p, \lambda, m)$ the scattering and absorption efficiencies. $Q_{\text{scat, abs}}(D_p, \lambda, m)$ were calculated using Mie scattering calculations described by Bohren and Huffman (1983). To compare with the measured σ_{scat}, all calculated values were corrected for the sample temperature and pressure, as well as for angular truncation examined for the nephelometer, taking into account the nephelometer geometry, integrating the light scattering at scattering angles between 10° and 170°. The uncertainties of σ_{scat} were estimated from these corrections on the order of 5.6 % in σ_{scat}. Since ammonium sulfate particles were assumed to be spherical (Pruppacher and Klett, 1996), mobility diameters are identical to geometrical diameter. Therefore, the mobility diameters measured by SMPS was directly used for the calculations. Number size distributions obtained with the SMPS were fitted with log-normal size distributions:

$$\frac{dN}{d\log D_p} = \frac{N_{tot}}{\sqrt{2\pi}\log\sigma} \exp\left[-\frac{\left(\log D_p - \log D_{p,g}\right)^2}{2(\log\sigma)^2} \right] \quad (2)$$

where N_{tot} is the integrated number concentration, σ is the standard deviation and $D_{p,g}$ is the fitted geometric diameter.

The optimized CRI was determined so that the difference between measured σ_{scat} and σ_{abs} and those obtained using Mie calculations was minimized. The uncertainties

AMTD
6, 6935–6974, 2013

were estimated from the σ_{scat} values obtained using Eq. (1) included in the uncertainties of σ_{scat} measurements.

In addition, the CRI in the visible was derived by comparing mobility size distributions obtained by the SMPS and optical size distributions measured simultaneously with the white light OPC. The optical size distributions were corrected for various CRI according to the manufacturer calibration curves. The CRI was determined so that the optical size distributions match with those retrieved from SMPS measurements (Heim et al., 2008; Hand and Kreidenweis, 2002). While the Welas instrument is considered to provide size distribution down to 150 nm, considering the decreased efficiency below 300 nm, this last value was adopted as the lower border of the studied range. By identifying the best calibration curves, the CRI in the visible range was obtained for aerosol size range from 300 to 500 nm. The uncertainties in retrieved CRI were determined from the difference between the DMA and OPC size distributions.

3.2 Determination of the size and scattering growth factor

The GF of monodisperse and polydisperse size distributions were derived from the H-TDMA and SMPS measurements respectively by assuming a lognormal profile as described in Sect. 3.1. GF is described by the relative increase in the geometric diameter of particles due to water uptake at a specific RH:

$$\mathrm{GF}(\mathrm{RH}) = \frac{D_{\mathrm{p,m}}(\mathrm{RH})}{D_{\mathrm{p,m}}(\mathrm{dry})} \quad (3)$$

Where $D_{\mathrm{p,m}}(\mathrm{RH})$ is the measured geometric diameter at a specific RH and $D_{\mathrm{p,m}}(\mathrm{dry})$ is the geometric diameter at low RH considered correspond to dry conditions (RH < 30 %). Uncertainties in GF were based on the uncertainties in particle size distributions that included DMA classification and calibration, as well as uncertainties in the estimation of $D_{\mathrm{p,m}}$ from size distributions. The measured GF were compared with theoretical calculations according to the model of Biskos et al. (2006) based on the Köhler equations.

AMTD
6, 6935–6974, 2013

The humidification in the chamber was performed for polydisperse size distributions that include a fraction of particles smaller than 100 nm (Fig. 3). Due to Kelvin effect, the water activity and hence the GF vary with size for particle size above 100 nm. Thus, a correction for the Kelvin effect was included in the theoretical calculation for the comparison with the SMPS measurements (Biskos et al., 2006).

Additionally, changes of the aerosol scattering properties due to hygroscopic growth were followed with the nephelometer and are represented by the ratio of the scattering coefficient at a specific RH σ_{scat}(RH) to the dry scattering coefficient σ_{scat}(dry):

$$f\,(\mathrm{RH}) = \frac{\sigma_{scat}(\mathrm{RH})}{\sigma_{scat}(\mathrm{dry})} \tag{4}$$

A 2 °C sample heating has been observed in the cell of the nephelometer in comparison to the sample inlet. Heating in nephelometers has already been observed in previous laboratory studies and can cause a reduction of the sample RH and thus an underestimation of f(RH) (Kus et al., 2004; Dougle et al., 1998; ten Brink et al., 2000). The consequences of this artifact will be discussed in Sect. 4.3. A correction for the sample RH was applied using the measured sample inlet RH sensor and the measured sample temperature within the cell. The dependence of the saturation vapor pressure of water on temperature is given by the empirical expression (Hinds, 1999):

$$P_s\,(T) = \exp\left[16.7 - \frac{4060}{(T-37)}\right] \tag{5}$$

where T is the temperature and P_s the saturated vapor pressure. Assuming a constant amount of water vapor, the RH changes of the sample due to increasing temperature in the cell of the nephelometer can be calculated as follows:

$$\frac{\mathrm{dRH}}{\mathrm{d}T} = \frac{-4060\mathrm{RH}}{(T-37)^2} \tag{6}$$

The f(RH) uncertainties were based on the scattering coefficient uncertainties and both the temperature and RH correction uncertainties.

AMTD
6, 6935–6974, 2013

4 Results

4.1 Refractive index of dry ammonium sulfate particles

The aethalometer response to ammonium sulfate particles was very small and thus the absorption spectrum of ammonium sulfate particles was considered negligible taking into account the calculation uncertainties. As a consequence, the retrieval procedure was conducted by fixing the imaginary part of the CRI equal to zero.

Figure 4 compares the σ_{scat} measured from nephelometer measurements at λ = 525 nm and those calculated from measured size distributions and Mie scattering calculations for various CRI. The value optimized of real part of the CRI value was determined to be 1.55(±0.02) which within the estimated uncertainties minimizes differences between measurements and calculations.

The real part of the CRI in the visible was also retrieved by overlapping size distributions from SMPS and those of an OPC. Figure 5 shows the optical size distributions corrected for various CRI and the corresponding mobility size distributions. For particles larger than 350 nm, the SMPS spectrum was found to agree well with the white light spectrum by using a CRI of $1.54 + 0i$. However, there is no clear evidence of the optimal CRI that would provide the best fit for particles smaller than 350 nm. In the size range between 300 and 350 nm, the SMPS spectrum was found to be equally far away optical the Welas spectrum calculated with a RI of $1.54 + 0i$ and $1.60 + 0i$. As a result, the retrieved RI is $1.57(\pm0.03) + 0i$.

All CRI values obtained in this study along with values reported in the literature are shown in Table 2. The CRI values obtained with the two methods are consistent with each other within the estimated uncertainties. At λ = 525 nm, they are also in reasonable agreement with the literature values of $1.52 + 0i$ (Riziq, 2007), $1.52(\pm0.03) + 0i$ (Nakayama et al., 2010) and $1.52 – 1.54 + 0i$ (Toon et al., 1976). The CRI in the visible is slightly higher than the value of $1.52(\pm0.01) + 0i$ obtained by Flores et al. (2009). This difference may be due to the limited CRI available in the OPC that reduces the

AMTD
6, 6935–6974, 2013

accuracy of the retrieved CRI. However, the difference remains very low (though only by up to 3 %) and closely linked to the value obtained at λ = 525 nm.

4.2 Hygroscopic growth of selected size of particles measured with the H-TDMA

The humidogram of ammonium sulfate injected in the smog chamber was established for a selected dry size of 150 nm with the H-TDMA for each RH which range between 45 and 90 %. In Fig. 6, the results in this study are compared with theoretical calculations according to the model of Biskos et al. (2006) and with humidograms presented in the H-TDMA comparison study by Duplissy et al. (2009). At RH < 78 %, dry particles exist as crystalline phase and no change in their size has been observed. The deliquescence transition was observed at 78.9 ± 4.3 %, in agreement with data from Duplissy et al. (2009). Above this RH value, the size of ammonium sulfate particle increased sharply and a solution droplet was formed. In aqueous solution, the particle grew by absorbing water vapor with increasing RH to maintain equilibrium with the water vapor. The experimental growth factors agree well with the liquid phase theory and with other studies (Duplissy et al., 2009). The results show also the high precision of the H-TDMA in detecting small change in GF with increasing RH in small increments. Our instrument seems to provide accurate measurements of particle hygroscopic growth and deliquescence.

4.3 Hygroscopic growth of polydisperse size particles obtained during humidification in the chamber

The hygroscopic growth of polydisperse ammonium sulfate particles was obtained by exposing in-situ the particles to varying RH. Number size distributions of particles are shown in Fig. 8 as a function of the RH. Two RH scales were used: within the smog chamber as well as the RH within the SMPS. Indeed, a decrease of RH has been observed between the simulation chamber and both the nephelometer and the SMPS. The maximum decrease in the sample RH of 20 % was observed in the SMPS and

AMTD
6, 6935–6974, 2013

occurred for a RH of 100 % in the chamber. A small drying of 10 % was observed between CESAM and the cell of the nephelometer. The drying may be due to water transfer into the sample line as a result of the length of sample line's (about 1 m) between CESAM and the instruments. The figure shows that, for hydration up to 30 % RH, the geometric diameter of particles does not change. From 30 % RH, the particle's geometric diameter increases from 121 nm to 145 nm at 73 % RH, resulting in a GF of 1.2.

This hygroscopic behavior was also observed for σ_{scat} (Fig. 8). At 30 % RH, the σ_{scat} increases with RH suggesting possible chemical properties and/or size distribution changes. A change in the slope is observed at 76 % RH that could be attributed to the deliquescence of ammonium sulfate particles. Although curves exhibit the same trend, different values are observed for a specific RH. This can be explained by the fact that the size distribution of the aerosol in the chamber was slightly different from one experiment to another. In particular, the proportion of particles larger than 100 nm was changing resulting in changing capacity in absorbing water (Biskos et al., 2006) and hence varying the observed GF and f(RH).

As previously discussed in Sect. 3.2, the number size distributions and the proportion of particle size above 100 nm change according to the experiment, resulting in changes in either their GF and f(RH). For example, f(RH) in experiment E2904 is 1.6 for a dry geometric diameter of 70 nm compared to 2.2 for 100 nm geometric diameter in experiment E1212.

To rationalize these observations, the hygroscopic behavior of particles measured using both the humidified SMPS and nephelometer during the chamber humidification were compared through a modeling study. We have considered that particles would exhibit different mixing states before and after their deliquescence RH. Figure 9 shows the methodology we applied to predict GF and f(RH) as a function of RH.

After deliquescence, particles are considered to be transformed into an aqueous solution phase and the GF calculations are similar to those described in Sect. 3.2, based on Köhler equations. Dry particles and droplets were assumed to be homogeneous

AMTD
6, 6935–6974, 2013

spheres of uniform CRI. The CRI calculations were based on volume weighted refractive indices of ammonium sulfate and water:

$$n_{\text{aerosol}} = n_{\text{ammonium sulfate}} x_{\text{ammonium sulfate}} + n_{\text{water}} x_{\text{water}} \quad (7)$$

where $x_{\text{ammonium sulfate}}$ and x_{water} are respectively the volume fraction of ammonium sulfate and water. Mie scattering calculations for homogeneous spheres (Wiscombe, 1980) were used to determine the dry and humidified σ_{scat} for $\lambda = 525$ nm both from measured GF at a specific RH and CRI. The ratio of the humidified σ_{scat} to the dry σ_{scat} gives the theoretical f(RH).

To explain the hygroscopic behavior before deliquescence, we have made the assumption that ammonium sulfate particles would take up water in a shell-like structure. The scattering properties of this simple model can be described by the homogeneous coated sphere theory presented in Bohren and Huffman (1983). We assumed that particles are composed of a core that has the same CRI as ammonium sulfate and a water mantle. For the complex CRI of pure ammonium sulfate, we used the value retrieved in Sect. 4.1 at $\lambda = 525$ nm. We have assumed a constant ammonium sulfate core size distribution. Assuming the changes of size distributions result from water mantles uniformly coated on ammonium sulfate particles, changes of σ_{scat} were calculated from the observed thickness of the water mantle. We have also considered a model in which σ_{scat} together with the optical code were used to derive the thickness of the water mantle and thus the GF as a function of the RH.

The hygroscopic behavior of ammonium sulfate particles compared with model predictions is shown in Fig. 10. The comparison between f(RH) measurements and the model that assumed particles have deliquesced was possible for 73 % RH. It was considered that ammonium sulfate particles were surrounded by a shell of condensed water for RH until 60 %. Indeed, these ranges of values represent those that allow comparison between model and measurement due to the drying out of the sample between CESAM and the instruments. The f(RH) and GF measurements agree well with the model for RH above 80 %, suggesting that a solution droplet is formed.

AMTD
6, 6935–6974, 2013

The deliquescence of ammonium sulfate particles is found to occur at a RH equal to 76.2 ± 4.3 %, in agreement with results obtained with the H-TDMA (Sect. 4.2). Before the deliquescence point, f(RH) values are too low to allow a conclusive comparison between the measurement and the theoretical curve. However, GF curves are in agreement within measurement uncertainties.

5 Discussion

These results suggest that particles accumulate water far before deliquescence. This continuous absorption of water was not observed with our H-TDMA, as well as in several previous studies using this instrument (Duplissy et al., 2009; Gysel et al., 2001). There are three main differences between the H-TDMA and in the humidification in the chamber approaches: (1) particles would continue to grow during the humidification process in the chamber by coagulation. The coagulation rate of particles was calculated before the humidification by measuring the evolution of the particle's size. We observed an increase of 2 % per hour that cannot explain the change in their size observed during humidification. Furthermore, we found no significant decrease of the number concentration due to the coagulation of particles. (2) The hygroscopic behavior of polydisperse size distribution was studied by in-situ humidification instead of for one selected size of particles with the H-TDMA. Schuttlefield et al. (2007) discussed that large distribution of particles would result in a continuous growth due to the small particles deliquescing sooner than the large particles. Biskos et al. (2006) reported, however, no nanosize effect on the RH values of deliquescence. Additionally, we observed the size variation occurs for the overall size distributions, suggesting that there is no effect of the particles size. (3) The residence time for particle humidification was significantly longer for the in-situ humidification. It takes a few minutes in the chamber, instead of 15 s in the H-TDMA. Recently, the residence time for humidification in hygroscopic measurements have obtained more attention (Chan and Chan, 2005). It was highlighted that hygroscopic measurements can be compromised if particles have

AMTD
6, 6935–6974, 2013

not attained their equilibrium state in the measurements. These new findings under simulated atmospheric conditions can be supported by complementary laboratory results. Indeed, Schuttlefield et al. (2007) observed with attenuated total reflection Fourier transform infrared spectroscopy that water was continuously absorbed on ammonium sulfate particles from 3 % RH. The particles were allowed to equilibrate with water vapor for 20 min. Krueger et al. (2003) observed water uptake on NaCl particles prior to deliquescence with environmental scanning electron microscope. In particular, at 75 % RH, they found that over a 35 min time of period particles become more spherical, although a solid NaCl core was remained. Trainic et al. (2012) also showed that ammonium sulfate particles exposed to varying RH from 30 % to 90 % RH during 1 h, and then dried, exhibit a trend of increasing growth in size. The results indicate that care need to be taken of the equilibrium time for water uptake in investigating the aerosols hygroscopic properties. H-TDMA instruments induce limited residence time for humidification that seems to be insufficient for water adsorption on ammonium sulfate particles.

6 Atmospheric implications

Our results suggest that the absorption of water by ammonium sulfate particles occurs well below the deliquescence point in a RH ranged from 30 to 80 %, which is common in most environments. The humidification was performed during few minutes that may be of relevance of the aerosols transport in the atmosphere. The deliquescence of ammonium sulfate particles occurs at 80 % RH and upon dehydration the particles exists as a solution droplets until 30 % RH. In consequence, depending on their RH history, ammonium sulfate particles may be surrounded by water layers or exist as an aqueous solution over a broad region for a wide range of RH values ranging from 30 to 80 %.

The water uptake implies a continuous change of size and chemical composition with increasing RH. The implication of this observation is important in that it alters the scattering properties. Many of the previous studies postulated that ammonium sulfate

AMTD
6, 6935–6974, 2013

particles have prompt deliquescence with no continuous hygroscopic growth below their deliquescence point (Tang, 1996; Cruz and Pandis, 2000; Gysel et al., 2001; Duplissy et al., 2009). In regards with the results obtained in this study, this assumption would underestimate the predicted cooling at the Earth's surface due to scattering by aerosols. However, in order to estimate quantitatively the impact of the water uptake on the sulfate radiative effect, the hygroscopic behavior of ammonium sulfate particles need to be inserted in a radiative code of a global circulation model.

The implication for heterogeneous chemistry may also be significant. Dry ammonium sulfate particles have been found to be highly unreactive to N_2O_5 (Mozurkewich and Calvert, 1988). However, small loss of N_2O_5 was observed on liquid ammonium sulfate particles (Hu and Abbatt, 1997). Knipping et al. 2000 also showed that kinetics of many heterogeneous reactions depend on the phase of particles. Therefore, the water layer on ammonium sulfate particles surface would have important consequence in the gas-particle partitioning of organic compounds, contributing to the Secondary Organic Aerosols formation (SOA). Kroll et al. (2005) observed that reactive uptake of glyoxal on aqueous seed contributes significantly to particle growth. Volkamer et al. (2009) also found SOA formation from glyoxal in the presence of ammonium sulfate particles at high RH.

7 Conclusions

A new approach was devised to allow an accurate description of the size, the properties and the hygroscopic behavior of particles. The CRI of aerosols was retrieved at one specific wavelength and also in the visible spectrum. The hygroscopic behavior of the polydisperse aerosols was obtained at RH values up to 100 % by measuring the change of the size and scattering coefficient due to water uptake. To validate the retrieved parameters, the CRI, the GF and the f(RH) of the ammonium sulfate particles were measured and compared with the literature, as well as with theoretical calculations based on Köhler and Mie theories.

AMTD
6, 6935–6974, 2013

The dry CRI of ammonium sulfate particles obtained from both methods compared favorably to each other and are also in reasonable agreement with the literature values.

The GF derived from the hygroscopic measurements were compared to values obtained for one selected size of particles with the H-TDMA. We have shown the importance of the residence time for water uptake in investigating the hygroscopic properties of aerosols. A continuous increase of the ammonium sulfate particle's size and light scattering was observed from RH values as low as 30 % RH when the humidification was performed in the chamber for a few minutes. Comparison of measured and modeled values of growth factors suggests that monolayers of water were adsorbed on ammonium sulfate particles below the deliquescence point. The water uptake on ammonium sulfate particles alters their scattering properties and may affect their radiative properties. In contradiction, the hygroscopic growth factor reported with the H-TDMA in this paper and in the literature showed that a prompt deliquescence of ammonium sulfate particles with no continuous growth in size at low RH.

The results highlights that the methodology established in the simulation chamber is a highly suitable approach to investigate the aerosols properties. Similar studies can be extended to many other aerosols. In particular, further studies are needed to measure the hygroscopic behavior of inorganic salt particles that exhibited prompt deliquescence in previous H-TDMA measurements (NaCl, Na_2SO_4, ...). Furthermore, the properties of aerosols with various size distributions should be investigated.

Acknowledgements. This research work has been supported by the European Community within the seventh Framework Programme: Eurochamp-2 (EU-FP7 grant agreement n°228335). The authors want to thanks George Biskos and Barbounis Konstantinos for their help in the development of the H-TDMA.

The publication of this article is financed by CNRS-INSU.

References

Abo Riziq, A., Trainic, M., Erlick, C., Segre, E., and Rudich, Y.: Extinction efficiencies of coated absorbing aerosols measured by cavity ring down aerosol spectrometry, Atmos. Chem. Phys., 8, 1823–1833, doi:10.5194/acp-8-1823-2008, 2008.

Albrecht, B. A.: Aerosols, cloud microphysics, and fractional cloudiness, Science, 245, 1227–1230, 1989.

Arnott, W. P., Hamasha, K., Moosmuller, H., Sheridan, P. J., and Ogren, J. A.: Towards aerosol light-absorption measurements with a 7-wavelength aethalometer: evaluation with a photoacoustic instrument and 3-wavelength nephelometer, Aerosol Sci. Tech., 39, 17–29, 2005.

Beaver, M. R., Garland, R. M., Hasenkopf, C. A., Baynard, T., Ravishankara, A. R., and Tolbert, M. A.: A laboratory investigation of the relative humidity dependence of light extinction by organic compounds from lignin combustion, Environ. Res. Lett., 3, 045003, doi:10.1088/1748-9326/3/4/045003, 2008.

Biskos, G., Paulsen, D., Russell, L. M., Buseck, P. R., and Martin, S. T.: Prompt deliquescence and efflorescence of aerosol nanoparticles, Atmos. Chem. Phys., 6, 4633–4642, doi:10.5194/acp-6-4633-2006, 2006.

Bohren, C. F. and Huffman, D. R.: Absorption and Scattering of Light by Small Particles, Wiley, New York, 1983.

Cappa, C. D., Lack, D. A., Burkholder, J. B., and Ravishankara, A. R.: Bias in filter-based aerosol light absorption measurements due to organic aerosol loading: evidence from laboratory measurements, Aerosol Sci. Tech., 42, 1022–1032, 2008.

Chan, M. N. and Chan, C. K.: Mass transfer effects in hygroscopic measurements of aerosol particles, Atmos. Chem. Phys., 5, 2703–2712, doi:10.5194/acp-5-2703-2005, 2005.

Charlson, R. J., Schwartz, S. E., Hales, J. M., Cess, R. D., Coakley, J. A., Hansen, J. E., and Hofmann, D. J.: Climate forcing by anthropogenic aerosols, Science, 255, 423–430, 1992.

Covert, D. S., Charlson, R. J., and Ahlquist, N. C.: A study of the relationship of chemical composition and humidity to light scattering by aerosols, J. Appl. Meteorol., 11, 968–976, 1972.

Cruz, C. N. and Pandis, S. N.: Deliquescence and hygroscopic growth of mixed inorganic-organic atmospheric aerosol. Environ. Sci. Technol., 34, 4313–4319, 2000.

Cubison, M. J., Coe, H., and Gysel, M.: A modified hygroscopic tandem DMA and a data retrieval method based on optimal estimation, J. Aerosol Sci., 36, 846–865, 2005.

AMTD
6, 6935–6974, 2013

Dinar, E., Riziq, A. A., Spindler, C., Erlick, C., Kiss, G., and Rudich, Y.: The complex refractive index of atmospheric and model humiclike substances (HULIS) retrieved by a cavity ring down aerosol spectrometer (CRD-AS), Faraday Discuss., 137, 279–295, 2008.

Dougle, P. G., Veefkind, J. P., and ten Brink, H. M.: Crystallisation of mixtures of ammonium nitrate, ammonium sulphate and soot, J. Aerosol Sci., 29, 375–386, 1998.

Duplissy, J., Gysel, M., Alfarra, M. R., Dommen, J., Metzger, A., Prevot, A. S. H., Weingartner, E., Laaksonen, A., Raatikainen, T., Good, N., Turner, S. F., McFiggans, G., and Baltensperger, U.: Cloud forming potential of secondary organic aerosol under near atmospheric conditions, Geophys. Res. Lett., 35, L03818, doi:10.1029/2007GL031075, 2008.

Duplissy, J., Gysel, M., Sjogren, S., Meyer, N., Good, N., Kammermann, L., Michaud, V., Weigel, R., Martins dos Santos, S., Gruening, C., Villani, P., Laj, P., Sellegri, K., Metzger, A., McFiggans, G. B., Wehrle, G., Richter, R., Dommen, J., Ristovski, Z., Baltensperger, U., and Weingartner, E.: Intercomparison study of six HTDMAs: results and recommendations, Atmos. Meas. Tech., 2, 363–378, doi:10.5194/amt-2-363-2009, 2009.

Flores, J. M., Trainic, M., Borrmann, S., and Rudich, Y.: Effective broadband refractive index retrieval by a white light optical particle counter, Phys. Chem. Chem. Phys., 11, 7943–7950, 2009.

Forster, P., Ramaswamy, V., Artaxo, P., Berntsen, T., Betts, R., Fahey, D. W., Haywood, J., Lean, J., Lowe, D. C., Myhre, G., Nganga, J., Prinn, R., Raga, G., Schulz, M., and Van Dorland, R.: Radiative Forcing of Climate Change, in: Climate Change 2007: The Physical Science Basis, Contribution of Working Group I to the Fourth Assessment Report of the Intergovernmental Panel on Climate Change, edited by: Solomon, S., Qin, D., Manning, M., Chen, Z., Marquis, M., Averyt, K. B., Tignor, M., and Miller, H. L., 2007.

Garland, R. M., Ravishankara, A. R., Lovejoy, E. R., Tolbert, M. A., and Baynard, T.: Parameterization for the relative humidity dependence of light extinction: organic-ammonium sulfate aerosol, J. Geophys. Res., 112, D19303, doi:10.1029/2006JD008179, 2007.

Gysel, M., Weingartner, E., and Baltensperger, U.: Hygroscopicity of aerosol particles at low temperatures, 2. theoretical and experimental hygroscopic properties of laboratory generated aerosols, Environ. Sci. Technol., 36, 63–68, 2001.

Gysel, M., Crosier, J., Topping, D. O., Whitehead, J. D., Bower, K. N., Cubison, M. J., Williams, P. I., Flynn, M. J., McFiggans, G. B., and Coe, H.: Closure study between chemical composition and hygroscopic growth of aerosol particles during TORCH2, Atmos. Chem. Phys., 7, 6131–6144, doi:10.5194/acp-7-6131-2007, 2007.

AMTD
6, 6935–6974, 2013

Hämeri, K., Väkevä, M., Hansson, H.-C., and Laaksonen, A.: Hygroscopic growth of ultrafine ammonium sulphate aerosol measured using an ultrafine tandem differential mobility analyzer, J. Geophys. Res., 105, 22231–22242, 2000.
Hand, J. L. and Kreidenweis, S. M.: A new method for retrieving particle refractive index and effective density from aerosol size distribution data, Aerosol Sci. Tech., 36, 1012–1026, 2002.
Hansen, J., Sato, M., and Ruedy, R.: Radiative forcing and climate response, J. Geophys. Res. Atmos., 102, 6831–6864, 1997.
Haywood, J. M. and Ramaswamy, V.: Global sensitivity studies of the direct radiative forcing due to anthropogenic sulfate and black carbon aerosols, J. Geophys. Res., 103, 6043–6058, 1998.
Haywood, J. M., Schwarzkopf, M. D., and Ramaswamy, V.: Estimates of radiative forcing due to modeled increases in tropospheric ozone, J. Geophys. Res., 103, 16999–17007, 1998.
Hegg, D., Larson, T., and Yuen, P. F.: A theoretical-study of the effect of relative-humidity on light scattering by tropospheric aerosols, J. Geophys. Res. Atmos., 98, 18435–18439, 1993.
Heim, M., Mullins, B. J., Umhauer, H., and Kasper, G.: Performance evaluation of three optical particle counters with an efficient multimodal calibration method, J. Aerosol Sci., 39, 1019–1031, 2008.
Henry, K. M. and Donahue, N. M.: Photochemical aging of alpha-pinene secondary organic aerosol: effects of oh radical sources and photolysis, J. Phys. Chem. A, 116, 5932–5940, 2012.
Hinds, W. C.: Aerosol Technology: Properties, Behavior, and Measurement of Airborne Particles, Book, 1999.
Hu, J. H. and Abbatt, J. P. D.: Reaction probabilities for N_2O_5 hydrolysis on sulfuric acid and ammonium sulfate aerosols at room temperature, J. Phys. Chem. A, 101, 871–878, 1997.
Huff Hartz, K. E., Rosenorn, T., Ferchak, S. R., Raymond, T. M., Bilde, M., Donahue, N. M., and Pandis, S. N.: Cloud condensation nuclei activation of monoterpene and sesquiterpene secondary organic aerosol, J. Geophys. Res., 110, D14208, doi:10.1029/2004JD005754, 2005.
Johnson, G. R., Fletcher, C., Meyer, N., Modini, R., and Ristovski, Z. D.: A robust, portable H-TDMA for field use, J. Aerosol Sci., 39, 850–861, 2008.
Knipping, E. M., Lakin, M. J., Foster, K. L., Jungwirth, P., Tobias, D. J., Gerber, R. B., Dabdub, D., and Finlayson-Pitts, B. J.: Experiments and simulations of ion-enhanced interfacial chemistry on aqueous NaCl aerosols, Science, 288, 301–306, 2000.

AMTD
6, 6935–6974, 2013

Kroll, J. H., Ng, N. L., Murphy, S. M., Varutbangkul, V., Flagan, R. C., and Seinfeld, J. H.: Chamber studies of secondary organic aerosol growth by reactive uptake of simple carbonyl compounds, J. Geophys. Res. Atmos., 110, D23207, doi:10.1029/2005JD006004, 2005.
Krueger, B. J., Grassian, V. H., Iedema, M. J., Cowin, J. P., and Laskin, A.: Probing heterogeneous chemistry of individual atmospheric particles using scanning electron microscopy and energy-dispersive X-Ray analysis, Anal. Chem., 75, 5170–5179, 2003.
Kus, P., Carrico, C., Rood, M., and Williams, A.: Measured and modeled light scattering values for dry and hydrated laboratory aerosols, J. Atmos. Ocean. Tech., 21, 981–994, 2004.
Liu, B. Y. H., Pui, D. Y. H., Whitby, K. T., and Kittelson, D. B.: The aerosol mobility chromatograph: a new detector for sulfuric acid aerosols, Atmos. Environ., 12, 99–104, 1978.
Liu, X., Cheng, Y., Zhang, Y., Jung, J., Sugimoto, N., Chang, S.-Y., Kim, Y. J., Fan, S., and Zeng, L.: Influences of relative humidity and particle chemical composition on aerosol scattering properties during the 2006 PRD campaign, Atmos. Environ., 42, 1525–1536, 2008.
Lohmann, U. and Feichter, J.: Global indirect aerosol effects: a review, Atmos. Chem. Phys., 5, 715–737, doi:10.5194/acp-5-715-2005, 2005.
Malm, W. C., Day, D. E., Kreidenweis, S. M., Collett, J., Jeffrey, L., Carrico, C., McMeeking, G., and Lee, T.: Hygroscopic properties of an organic-laden aerosol, Atmos. Environ., 39, 4969–4982, 2005.
Martin, S. T.: Phase transitions of aqueous atmospheric particles, Chem. Rev., 100, 3403–3453, 2000.
Meyer, N. K., Duplissy, J., Gysel, M., Metzger, A., Dommen, J., Weingartner, E., Alfarra, M. R., Prevot, A. S. H., Fletcher, C., Good, N., McFiggans, G., Jonsson, Å. M., Hallquist, M., Baltensperger, U., and Ristovski, Z. D.: Analysis of the hygroscopic and volatile properties of ammonium sulphate seeded and unseeded SOA particles, Atmos. Chem. Phys., 9, 721–732, doi:10.5194/acp-9-721-2009, 2009.
Mozurkewich, M. and Calvert, J. G.: Reaction probability of N_2O_5 on aqueous aerosols, J. Geophys. Res.-Atmos., 93, 15889–15896, 1988.
Nakayama, T., Matsumi, Y., Sato, K., Imamura, T., Yamazaki, A., and Uchiyama, A.: Laboratory studies on optical properties of secondary organic aerosols generated during the photooxidation of toluene and the ozonolysis of alphapinene, J. Geophys. Res.-Atmos., 115, D24204, doi:10.1029/2010JD014387, 2010.

AMTD
6, 6935–6974, 2013

Nemesure, S., Wagener, R., and Schwartz, S. E.: Direct shortwave forcing of climate by the anthropogenic sulfate aerosol: sensitivity to particle size, composition, and relative humidity, J. Geophys. Res. Atmos., 100, 26105–26116, 1995.
Nilsson, E., Swietlicki, E., Sjogren, S., Löndahl, J., Nyman, M., and Svenningsson, B.: Development of an H-TDMA for long-term unattended measurement of the hygroscopic properties of atmospheric aerosol particles, Atmos. Meas. Tech., 2, 313–318, doi:10.5194/amt-2-313-2009, 2009.
Orr Jr., C., Hurd, F. K., and Corbett, W. J.: Aerosol size and relative humidity, J. Coll. Sci., 13, 472–482, 1958.
Petters, M. D., Wex, H., Carrico, C. M., Hallbauer, E., Massling, A., McMeeking, G. R., Poulain, L., Wu, Z., Kreidenweis, S. M., and Stratmann, F.: Towards closing the gap between hygroscopic growth and activation for secondary organic aerosol – Part 2: Theoretical approaches, Atmos. Chem. Phys., 9, 3999–4009, doi:10.5194/acp-9-3999-2009, 2009.
Prenni, A. J., DeMott, P. J., and Kreidenweis, S. M.: Water uptake of internally mixed particles containing ammonium sulfate and dicarboxylic acids, Atmos. Environ., 37, 4243–4251, 2003.
Pruppacher, H. and Klett, J. D.: Microphysics of Clouds and Precipitation, Book, 1996.
Ristovski, Z. D., Morawska, L., Hitchins, J., and Barron, W.: Influence of the sheath air humidity on the SMPS measurements of hygroscopic aerosols, J. Aerosol Sci., 29, S327–S328, 1998.
Saathoff, H., Naumann, K.-H., Schnaiter, M., Schöck, W., Mähler, O., Schurath, U., Weingartner, E., Gysel, M., and Baltensperger, U.: Coating of soot and $(NH_4)_2SO_4$ particles by ozonolysis products of α-pinene, J. Aerosol Sci., 34, 1297–1321, 2003.
Saxena, P., Hildemann, L. M., McMurry, P. H., and Seinfeld, J. H.: Organics alter hygroscopic behavior of atmospheric particles, J. Geophys. Res., 100, 18755–18770, 1995.
Schuttlefield, J., Al-Hosney, H., Zachariah, A., and Grassian, V. H.: Attenuated total reflection fourier transform infrared spectroscopy to investigate water uptake and phase transitions in atmospherically relevant particles, Appl. Spectrosc., 61, 283–292, 2007.
Sjogren, S., Gysel, M., Weingartner, E., Baltensperger, U., Cubison, M. J., Coe, H., Zardini, A. A., Marcolli, C., Krieger, U. K., and Peter, T.: Hygroscopic growth and water uptake kinetics of two-phase aerosol particles consisting of ammonium sulfate, adipic and humic acid mixtures, J. Aerosol Sci., 38, 157–171, 2007.
Svenningsson, I. B., Hansson, H. C., Wiedensohler, A., Ogren, J. A., Noone, K. J., and Hallberg, A. Hygroscopic growth of aerosol-particles in the Po Valley, Tellus B, 44, 556–569, 1992.

AMTD
6, 6935–6974, 2013

Swietlicki, E. and Hansson, H.-C.: Hygroscopic properties of submicrometer atmospheric aerosol particles measured with H-TDMA instruments in various environments – a review, Tellus B, 60, 432–469, 2008.

Tang, I. N.: Chemical and size effects of hygroscopic aerosols on light scattering coefficients, J. Geophys. Res., 101, 19245–19250, 1996.

ten Brink, H. M., Khlystov, A., Kos, G. P. A., Tuch, T., Roth, C., and Kreyling, W.: A high-flow humidograph for testing the water uptake by ambient aerosol, Atmos. Environ., 34, 4291–4300, 2000.

Toon, O. B., Pollack, J. B., and Khare, B. N.: The optical constants of several atmospheric aerosol species: ammonium sulfate, aluminum oxide, and sodium chloride, J. Geophys. Res., 81, 5733–5748, 1976.

Trainic, M., Riziq, A. A., Lavi, A., and Rudich, Y.: Role of interfacial water in the heterogeneous uptake of glyoxal by mixed glycine and ammonium sulfate aerosols, J. Phys. Chem. A, 116, 5948–5957, 2012.

Tritscher, T., Dommen, J., DeCarlo, P. F., Gysel, M., Barmet, P. B., Praplan, A. P., Weingartner, E., Prévôt, A. S. H., Riipinen, I., Donahue, N. M., and Baltensperger, U.: Volatility and hygroscopicity of aging secondary organic aerosol in a smog chamber, Atmos. Chem. Phys., 11, 11477–11496, doi:10.5194/acp-11-11477-2011, 2011.

Van Dingenen, R., Putaud, J.-P., Martins-Dos Santos, S., and Raes, F.: Physical aerosol properties and their relation to air mass origin at Monte Cimone (Italy) during the first MINATROC campaign, Atmos. Chem. Phys., 5, 2203–2226, doi:10.5194/acp-5-2203-2005, 2005.

Varutbangkul, V., Brechtel, F. J., Bahreini, R., Ng, N. L., Keywood, M. D., Kroll, J. H., Flagan, R. C., Seinfeld, J. H., Lee, A., and Goldstein, A. H.: Hygroscopicity of secondary organic aerosols formed by oxidation of cycloalkenes, monoterpenes, sesquiterpenes, and related compounds, Atmos. Chem. Phys., 6, 2367–2388, doi:10.5194/acp-6-2367-2006, 2006.

Villani, P., Picard, D., Michaud, V., Laj, P., and Wiedensohler, A.: Design and validation of a volatility hygroscopic tandem differential mobility analyzer (VH-TDMA) to characterize the relationships between the thermal and hygroscopic properties of atmospheric aerosol particles, Aerosol Sci. Tech., 42, 729–741, 2008.

Volkamer, R., Ziemann, P. J., and Molina, M. J.: Secondary Organic Aerosol Formation from Acetylene (C_2H_2): seed effect on SOA yields due to organic photochemistry in the aerosol aqueous phase, Atmos. Chem. Phys., 9, 1907–1928, doi:10.5194/acp-9-1907-2009, 2009.

AMTD
6, 6935–6974, 2013

Wang, J., Doussin, J. F., Perrier, S., Perraudin, E., Katrib, Y., Pangui, E., and Picquet-Varrault, B.: Design of a new multi-phase experimental simulation chamber for atmospheric photosmog, aerosol and cloud chemistry research, Atmos. Meas. Tech., 4, 2465–2494, doi:10.5194/amt-4-2465-2011, 2011.

Weingartner, E., Gysel, M., and Baltensperger, U.: Hygroscopicity of aerosol particles at low temperatures, 1. new low-temperature H-TDMA instrument: setup and first applications, Environ. Sci. Technol., 36, 55–62, 2001.

Wex, H., Kiselev, A., Stratmann, F., Zoboki, J., and Brechtel, F.: Measured and modeled equilibrium sizes of NaCl and $(NH_4)_2SO_4$ particles at relative humidities up to 99.1 %, J. Geophys. Res., 110, 955–989, 2005.

Wex, H., Petters, M. D., Carrico, C. M., Hallbauer, E., Massling, A., McMeeking, G. R., Poulain, L., Wu, Z., Kreidenweis, S. M., and Stratmann, F.: Towards closing the gap between hygroscopic growth and activation for secondary organic aerosol: Part 1 – Evidence from measurements, Atmos. Chem. Phys., 9, 3987–3997, doi:10.5194/acp-9-3987-2009, 2009.

Wiscombe, W.: Improved Mie Scattering Algorithms, Appl. Optics, 19, 1505–1909, 1980.

Yoon, S.-C. and Kim, J.: Influences of relative humidity on aerosol optical properties and aerosol radiative forcing during ACE-Asia, Atmos. Environ., 40, 4328–4338, 2006.

AMTD
6, 6935–6974, 2013

Table 1. Summary of the experimental conditions for each experiment: Temperature, pressure, relative humidity in the chamber and the particles mass concentration injected in the chamber.

Experiment number	Temperature (K)	Pressure (mbar)	Relative Humidity (%)	$[particles]_{max}$ ($\mu g\,m^{-3}$)
E2904	298	1001	< 1	180
E3004	296	1005	< 1	140
E0305	293	1002	< 1	143
E2809	291	1010	< 1	266
E1212	294	1001	< 1	110

AMTD
6, 6935–6974, 2013

Table 2. Retrived RI of dry ammonium sulfate particles for λ = 525 nm and in the visible.

Experiment number	λ = 525 nm	visible
E2904	1.55 (±0.02) +0i	1.57 (±0.03) +0i
E3004	1.54 (±0.02) +0i	1.57 (±0.03) +0i
E0305	1.54 (±0.02) +0i	1.57 (±0.03) +0i
E2809	1.55 (±0.02) +0i	1.57 (±0.03) +0i
E1212	1.55 (±0.02) +0i	1.57 (±0.03) +0i
Literature	1.52 +0i[a] 1.52 (±0.03) +0i[b] 1.52–1.54 +0i[c]	1.52 (±0.01) +0i[d]

Values taken from [a] Riziq et al. (2007), [b] Nakayama et al. (2010), [c] Toon et al. (1976), and [d] Flores et al. (2009).

AMTD
6, 6935–6974, 2013

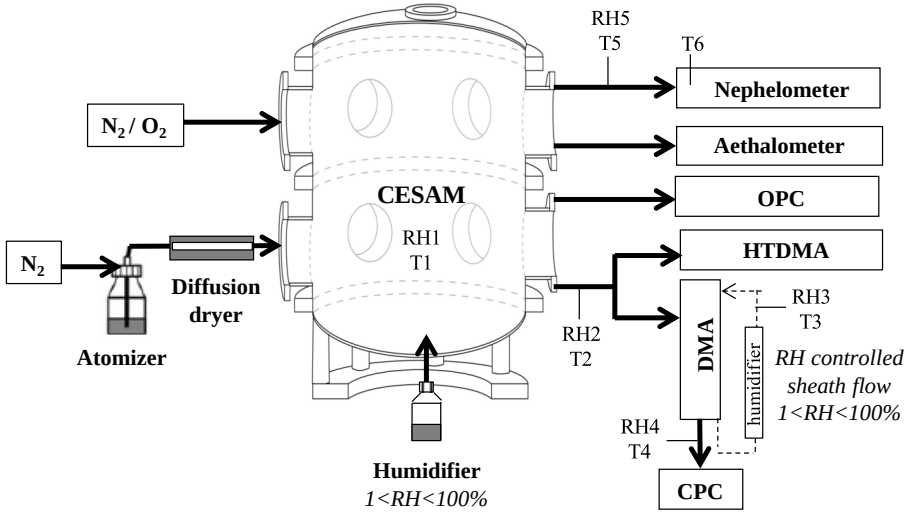

Fig. 1. Experimental set up used to measure aerosol hygroscopic and optical properties.

AMTD
6, 6935–6974, 2013

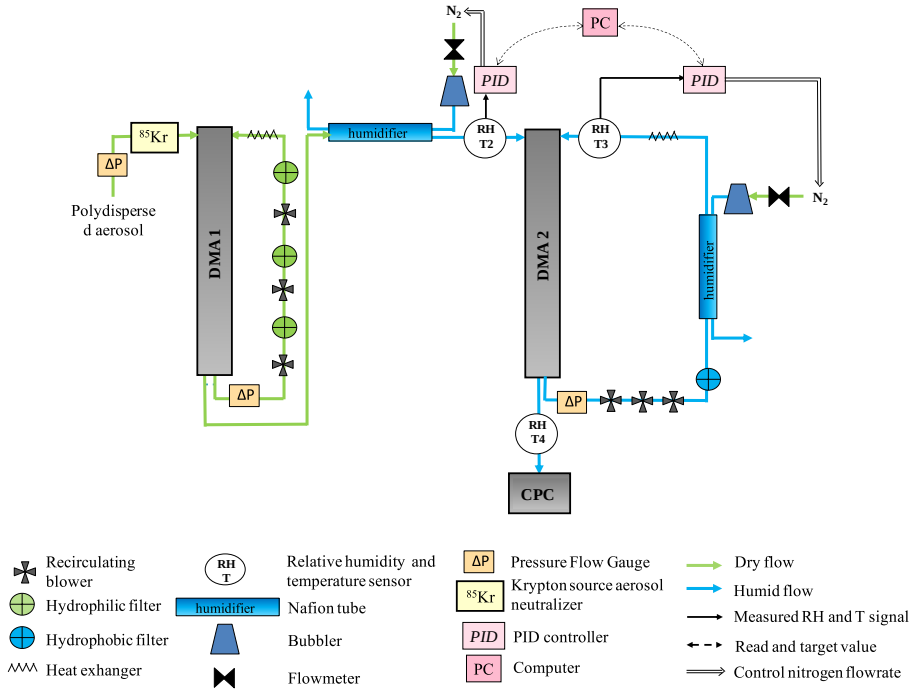

Fig. 2. Schematic diagram showing the layout of the H-TDMA.

AMTD
6, 6935–6974, 2013

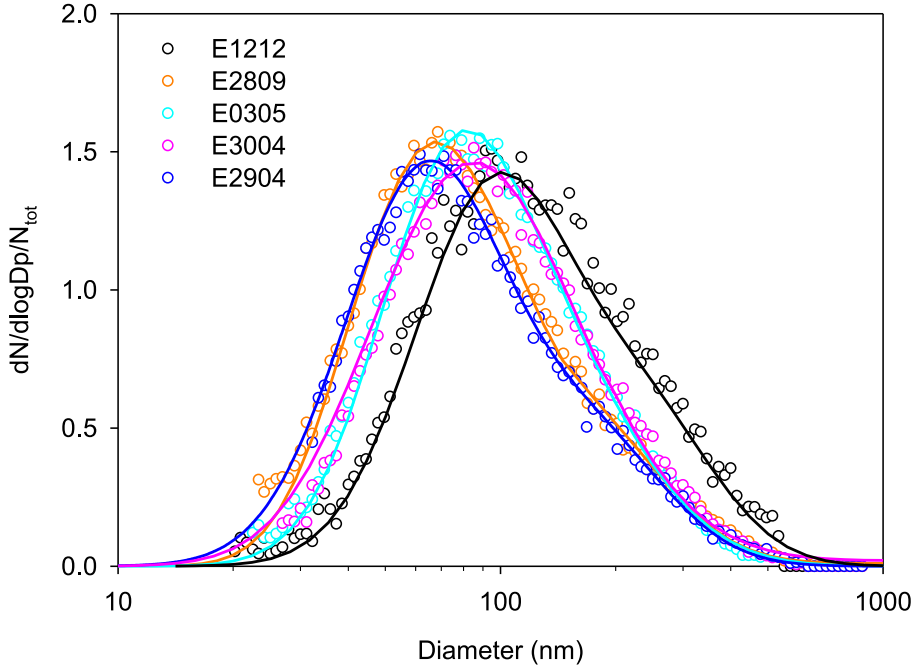

Fig. 3. Dry size distributions concentration for ammonium sulfate particles normalized by total number concentration (N_{tot}) in the smog chamber before the injection of water vapor.

AMTD
6, 6935–6974, 2013

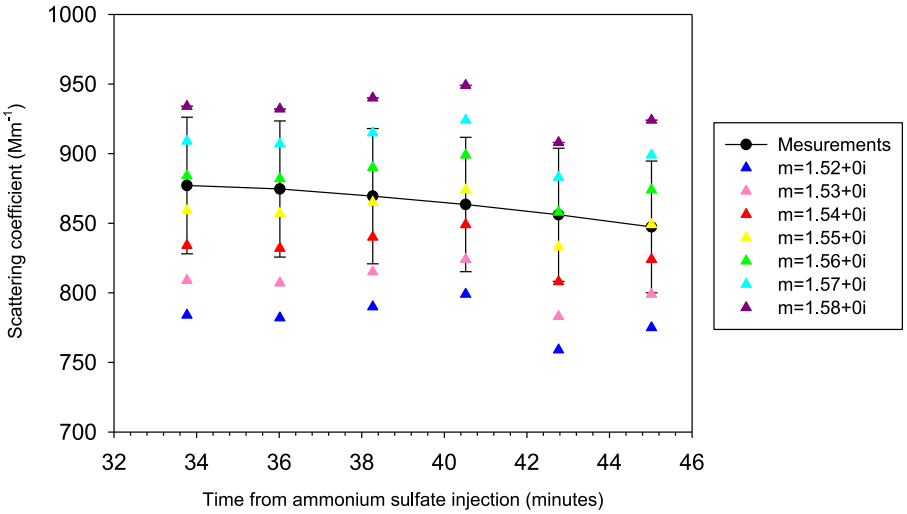

Fig. 4. Measured and calculated scattering coefficient using Mie scattering calculations for different CRI.

AMTD
6, 6935–6974, 2013

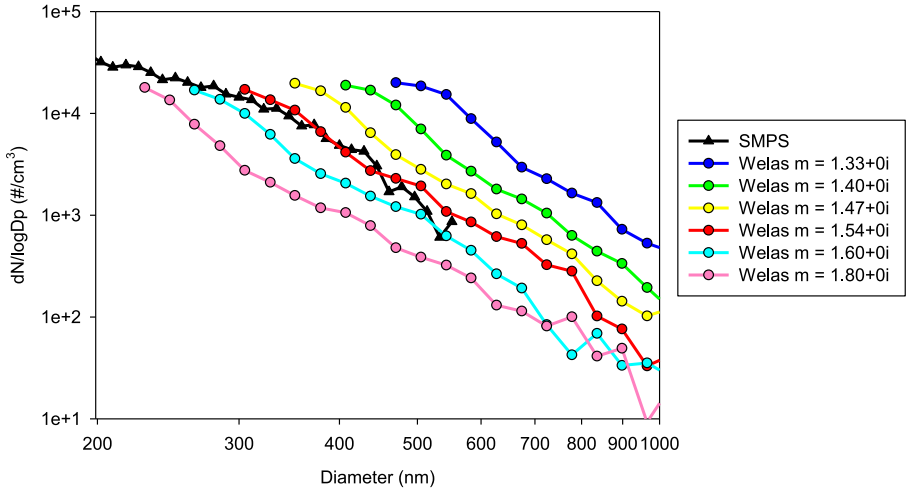

Fig. 5. Mobility size distribution (dark circles) and optical size distributions obtained for different CRI (colored circles).

AMTD
6, 6935–6974, 2013

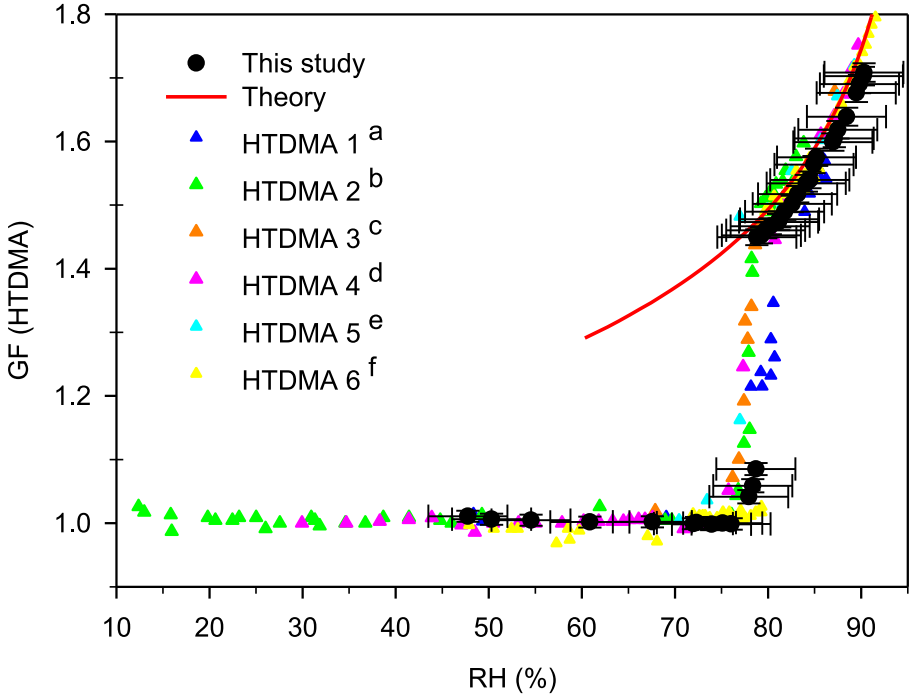

Fig. 6. Humidogram of 150 nm ammonium sulfate particles showing the hygroscopic growth factor measured with the H-TDMA as a function of relative humidity (black circle). The solid red line described the theory from Biskos et al. (2006). Humidograms from Duplissy et al. (2009) of were added for comparison (colored triangle). (a) Van Dingenen et al. (2005), (b) Weingartner et al. (2001); Gysel et al. (2002), (c) Villani et al. (2008), (d) Cubison et al. (2005); Gysel et al. (2007), (e) Johnson et al. (2008), (f) Duplissy et al. (2008).

AMTD
6, 6935–6974, 2013

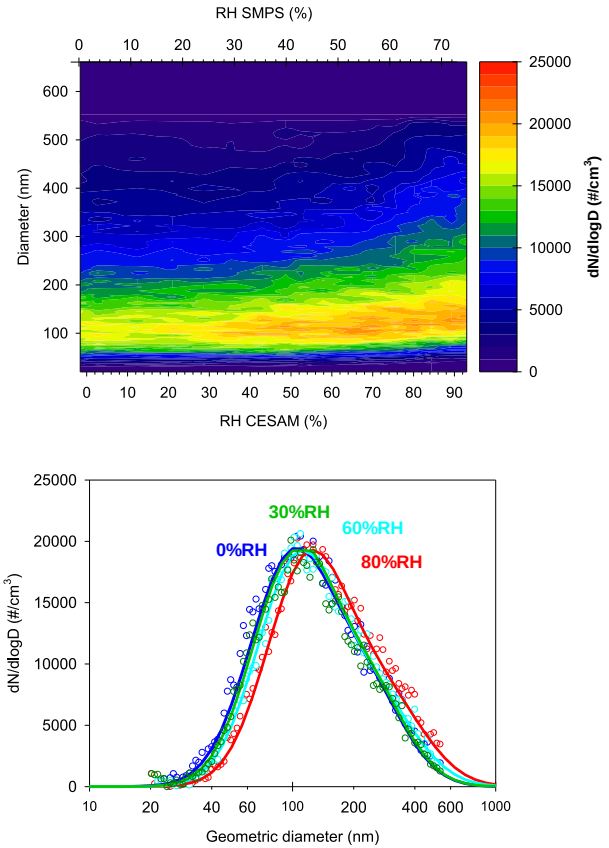

Fig. 7. Number size distribution of ammonium sulfate particles for increasing RH during humidification in the chamber in the experiment E1212.

AMTD
6, 6935–6974, 2013

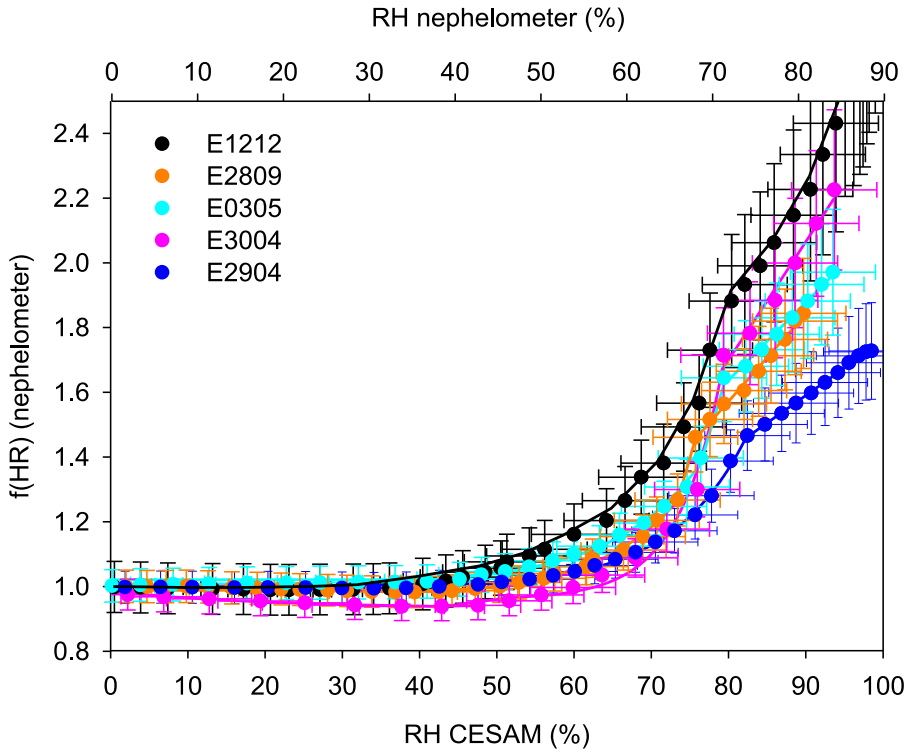

Fig. 8. Scattering growth factor *f* (RH) as a function of RH within the chamber (bottom axis) and the RH within the nephelometer (upper axis).

AMTD
6, 6935–6974, 2013

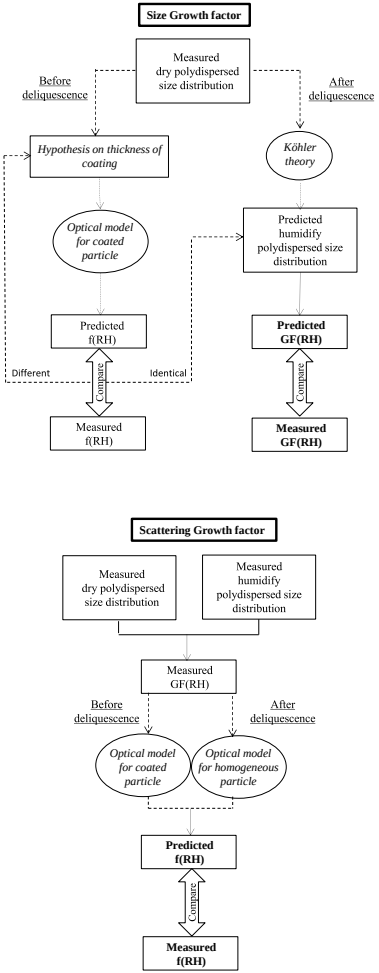

Fig. 9. Method used to compare measured and predicted size and scattering growth factor.

AMTD
6, 6935–6974, 2013

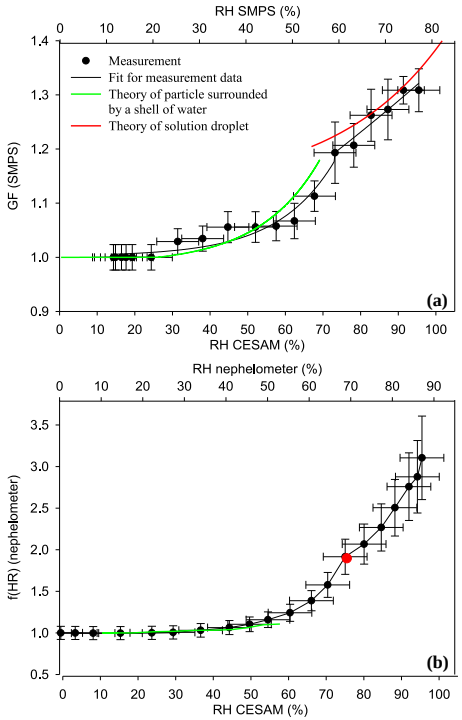

Fig. 10. Hygroscopic growth factor GF **(a)** and scattering growth factor f(RH) **(b)** as a function of RH within the chamber (bottom axis) and the RH within the measuring instrument (upper axis) obtained for the experiment E1212. The measurements are shown in black circles. The modeled growth factors based on the theory describing ammonium sulfate particle surrounded by a shell of water (red line) and solution droplet (green line) is also added. The black line represents a fit through data measurement.

AMTD
6, 6935–6974, 2013